Distortion and Overlay Performance of UV Step and Repeat Imprint Lithography

Jin Choi[1], Kevin Nordquist[2], Ashuman Cherala[1], Lester Casoose[3], Kathy Gehoski[2], William J. Dauksher[2], S.V. Sreenivasan[1‡], Douglas J. Resnick[2]

[1]*Molecular Imprints, Inc., Austin, Texas, USA*
[2] *Microelectronics and Physical Sciences Laboratories, Motorola Labs, Tempe, Arizona, USA*
[3]*Freescale Semiconductor, Tempe, Arizona, USA*

Abstract

High-resolution overlay is considered to be an important challenge for imprint lithography processes. A key advantage of Step and Flash™ Imprint Lithography (S-FIL™) is that it uses low-pressures (<1/40th of an atmosphere) at room temperature during the imprint processes. This makes it specifically suited for overlay as compared to other thermal or high pressure processes. To obtain high resolution overlay, it is critical to minimize in-plane distortions in both the template and substrate. This article presents a detailed budget of the various distortions that affect the S-FIL process. These distortions include i) 1X template e-beam pattern distortions, ii) template distortions due to post-processing steps, and iii) wafer processing distortions. Distortions associated with template patterning were measured prior to Cr removal using a Leica LMS tool. Field-to-field distortion variations were measured using 27 imprints on three wafers from a step and repeat imprint tool without control of thermal environment. Thermal effects on the imprint tool showed up as uniform magnification errors. Using the field-to-field distortion data, a first order correction scheme was implemented numerically to significantly lower the imprint-related distortion. Related issues such as XY-Theta alignment is also discussed briefly.

Keywords: Imprint Lithography; Overlay; S-FIL; Template distortion

‡*Corresponding Author: svs@militho.com; 515-339-7760; 1807 West Braker Ln, C-100, Austin TX 78758, U.S.A.*

1. Introduction

High-resolution overlay is considered to be an important challenge for nano imprint lithography processes[1,2,3]. Imprint processes can be grouped, generally, as hot embossing processes, where a spin-coated polymer is deformed according to patterns on a master under an elevated temperature above the glass-transition temperature (*Tg*) and high pressure [1], and UV imprint processes, where a low viscous fluid layer fills the master-substrate interface under room temperature and low pressure [2,3]. Recently imprint samples on 8" wafers using both technologies were presented by separate groups [4,5]. One of advantages of UV imprint processes as compared to other processes is its potential for superior overlay. To obtain high resolution overlay, it is critical to minimize the total in-plane distortions starting from the steps of the template patterning to final wafer patterning. This article presents a detailed budget of the various distortions that affect the UV imprint process. These distortions include i) 1X template e-beam pattern distortions, ii) template distortions due to post-processing steps, and iii) wafer processing distortions.

2. Template placement measurement

Figure 1 illustrates the template fabrication steps used for the S-FIL process[2]. Typically, four templates can be generated from a single 6025 substrate. Template pattern images can be generated by laser or e-beam patterning tools [6,7] and subsequently by etching tools to generate template features (Step 2) where a Cr layer is typically used as the etching mask. For the purpose of step and repeat, a step structure (mesa) is made by removing (etching) material from the surrounding area outside of the template active area (Step 3). Next, each template is diced from the substrate before it is cleaned and ready for imprint processes (Step 4). Dicing and mesa etching steps are considered as post-processing steps. These two post-processing steps can be

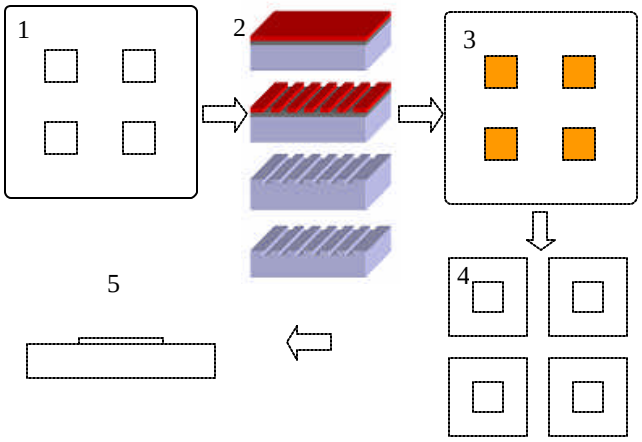

Figure 1: Template fabrication steps: 1. Substrate preparation for multiple templates; 2. E-beam patterning and etching; 3. Masking for mesa generation; 4. Mesa etching, Cr removal, and dicing ; 5. Final template side view

interchanged in practice and can potentially contribute to changes on the structural stress of the template along with the Cr removal step [6,7,8]. When the template substrate is supported via a three-point mounting scheme, up to 22.6nm of gravity attributable in-plane-distortion (IPD) was simulated and data were reported to be fairly insensitive to the pattern density of the template [9]. Recently, data of material properties of thin-film materials was presented [10] and it is believed that such data can be used to model the Cr removal effect more accurately as compared to the case of using conventional bulk material properties.

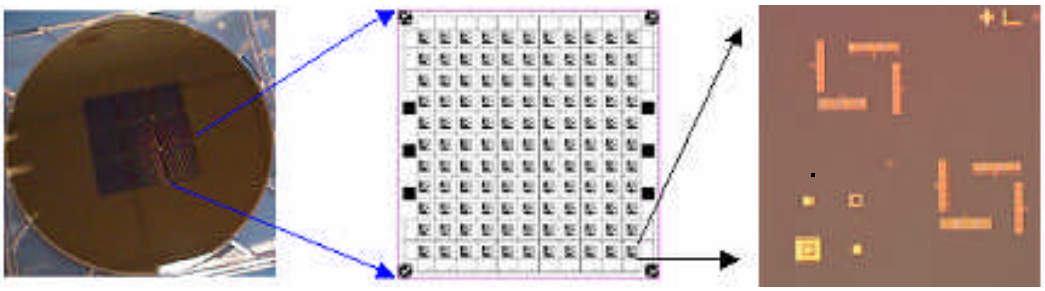

(a) (b) (c)

Figure 2. (a) 3 by 3 array imprints on a wafer. (b) Each 25mm square imprint contains 11 by 11 grid of in-plane placement targets (shown in a dotted circle in (c)).

For the purpose of template distortion measurement, four templates each containing an 11 by 11 grid of measurement targets were generated from a single 6025 substrate. Figure 2 (a) shows an imprinted wafer using a test template. The 11x11 array of placement targets is shown in Figure 2(b), and a magnified view of one target is shown in Figure 2 (c). The template placement data, shown in Figure 3, was measured using a Leica LMS IPro tool at DuPont Photomasks, Inc. prior to Cr stripping from the template. In this measurement, every other target was measured to generate a 6×6 grid of data. Scaling errors were x: –0.356ppm and y: 0.078ppm

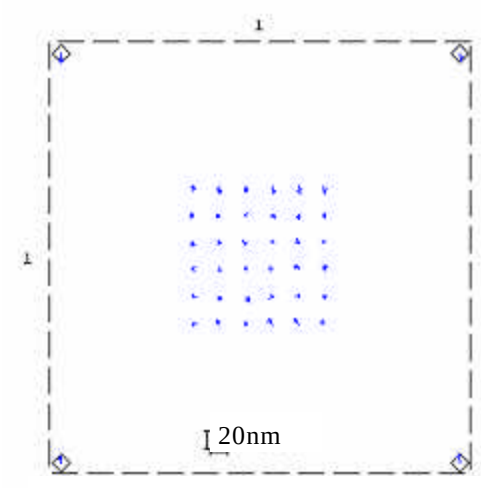

Figure 3 Template IPD prior to Cr removal (Courtesy of DuPont Photomasks, Inc). Edges of the 65mm template were also measured.

	No 1		No 2		No 3		No 4	
	x	y	x	y	x	y	x	y
Mean	0	-1	-1	-3	0	-3	-4	-3
Max e	-4	-9	-6	-10	-6	-11	-9	-12
Max 3 s	7	15	7	14	8	13	8	14

Table 1. Template IPD data (nm). Template No 1 was used for the experiments in the rest of this article.

(the scaling difference between x and y axes is 0.434ppm) and orthogonal error was 0.115 micro-radian. In-plane measurement data of four templates are summarized in Table 1. Template No 1 was used to generate imprint samples.

Now, the effects of template post-processing steps on the distortion of the active area are discussed. Before the mesa etching, the 6025 substrate was diced into separate templates. Due to the relatively smaller size of the template active area (25mm) as compared to the size of the template (65mm), no significant strain distortions are expected from the dicing step in the active area. Nordquista, et al. [7] reported that the removal of the Cr layer could cause 0.10 to 0.13 ppm shift from their resist feature placement. Therefore, assuming a +0.1 ppm increase in template dimensions in x and y due to Cr removal, it is estimated that the scale errors after Cr removal is approximately equal to -0.256ppm in x and ~0.178ppm in y. In the presence of non-uniformity of the pattern density, the Cr removal will cause a non-uniform IPD. However, it is expected that such a non-uniform IPD will be much smaller for a S-FIL template considering for its thickness (>6mm) as compared to the case of X-ray mask. Measuring the template after the post processing directly is in progress and data will be presented in the near future.

3. Distortions from wafer processing and template post processing

Imprint processes involve interaction forces where both the template and wafer may be conforming to each other. In S-FIL process, imprint forces are typically maintained below 1.5N for 25mm by 25mm templates. It is important to maintain the imprint force as low as possible while maintaining the template and wafer interface as uniform as possible. Typical imprint layer thickness and uniformity data from S-FIL process were presented by McMackin, et al [4]. The nature of the low imprinting force of S-FIL process can prevent any significant template-substrate deformations. Bending or deformation of the template can induce significant imprint in-plane distortions.

For the purposes of in-plane measurement, three wafers with nine imprints each were generated using Template No 1 (of Figure 3). Figure 2 illustrated one of three test wafers with nine imprints. Due to the optical imaging requirements associated with the LMS-2020 tool, imprint residual layers need to be maintained thin and uniform. In this experiment, good contrast was achieved with films having mean residual layers of 25nm with a 3σ variation of ~15nm. Otherwise, inconsistent image contrasts due to film thickness changes contribute to poor repeatability on the LMS-2020 tool. A total of 20 repetitive measurements were made on each of the 121 placement targets of one imprint to evaluate the LMS-2020 performance. Figure 4 shows that the LMS-2020 tool has a repeatability of <10nm 3 σ.

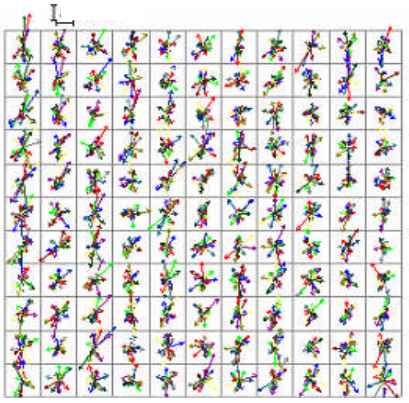

Summary	X[nm]	Y[nm]
Mean	0.00	-0.00
Max 3 S.D.	5.80	9.71
Min	-5.85	-10.92
Max	6.19	10.83

Figure 4. Repeatability test data with 20 repetitive measurements: <10nm 3 σ

Subsequently each of the 121 placement targets on each of the 27 imprints was read 5 times and an average

file was created of the 5 readings to minimize the measurement errors from the LMS-2020 tool. Due to the notch position of wafer, its measurement coordinates in Figure 4 are 90º rotated CW as compared to those of the template, shown in Figure 3.

3.1 Wafer to wafer process distortion

Figure 5 shows a wafer surface profile with nine imprints on the LMS-2020 tool. For a proper wafer to wafer distortion measurement, in addition to generating uniform imprints, errors associated with the LMS-2020 chuck flatness and backside particle problems had to be filtered by eliminating imprints and points where excessive z variations existed. All fields that created positive Z deflections = 250 nm were excluded from IPD measurement and all single data points were excluded from IPD measurement that created negative Z deflections = 250 nm.

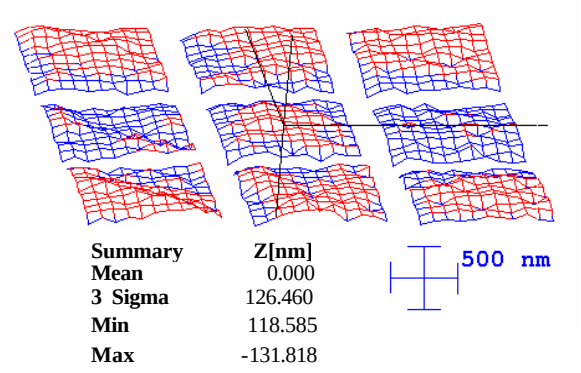

Figure 5. Surface profile of a wafer with nine imprints on LMS tool

Figure 6 shows a displacement error map between two wafers with field-to-field comparison (for e.g. the data (1,1) in Figure 6 is obtained by [wafer1(1,1) – wafer2(1,1)]. Even after the removal of data with >250nm Z deformation, there still remain a few local points showing effects that appear to be LMS-2020 chuck flatness problem or small back side particles of wafers. Generally, as shown in Figure 6, the largest in-plane overlay errors were in fields (1,1), (1,3), (2,1), and (3,3). The dominant component of the errors was measured as magnification errors. The imprint tool used for this experiment was not in a temperature-controlled unit with an environmental variation of as much as +/-1.5 degrees. Wafer temperature variation of ~+-0.5 degrees can induce the kind of mag errors noticed in Figure 6. This clearly

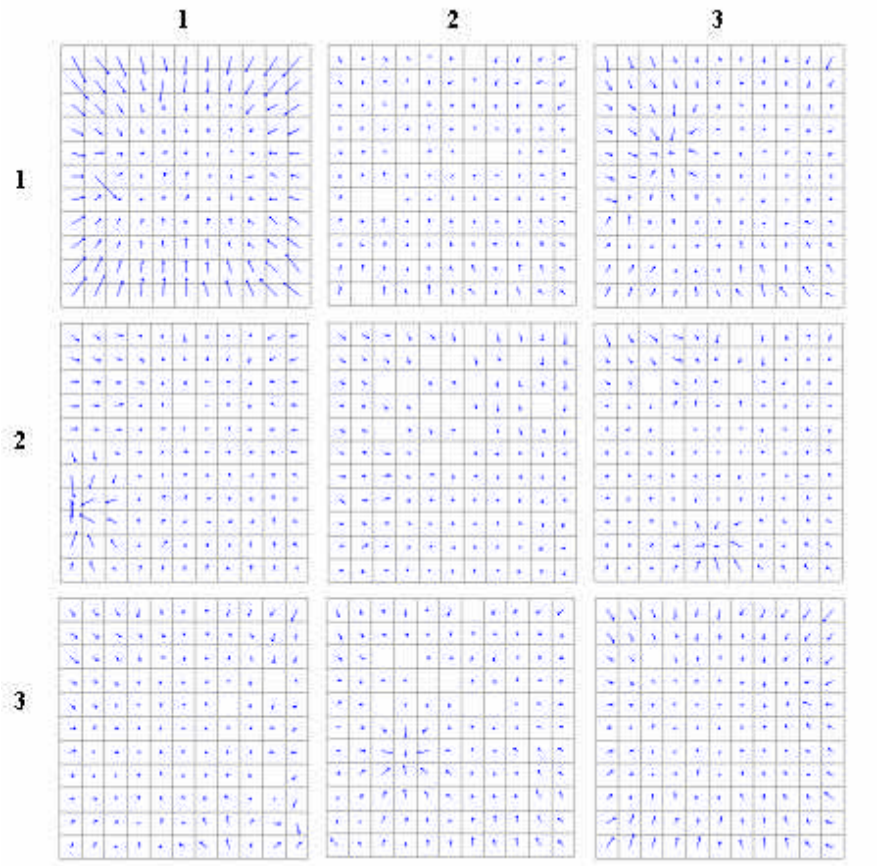

Die (R,C)	X (m+3s)	Y (m+3s)
1,1	42.91	55.49
1,2	9.49	19.18
1,3	20.44	29.84
2,1	23.81	27.95
2,2	16.40	8.8
2,3	18.21	18.69
3,1	17.51	18.9
3,2	15.73	22.76
3,3	20.02	28.44

Figure 6. Wafer to wafer comparison for each field. Majority of the overlay error is due to magnification difference.

shows that overall tool thermal management must be carefully maintained for the purpose of minimizing field-to-field mag errors. Such thermal control is a topic of ongoing research.

3.2 Template post processing distortion

Figure 7(a) shows the composite distortion map for all of the 27 fields. Figure 7(b) is a distortion map obtained by averaging the 27 fields and 7(c) is a distortion map after first order corrections (scale and orthogonality corrections) were applied on the map of 7(b). It was found to be difficult to measure placement data in chrome-less templates using the LMS-2020. Therefore, in this research, the map of Figure 7(b) was used as the distortion map of the post-processed template. Between Figures 7(b) and 7(c), scaling error was x: 1.48 ppm and y: 1.05 ppm and orthogonal error was -1.51 micro-radian. Compared to the distortion data of the template prior to the post-processing steps (Figure 3), Figure 7(c) shows that the 3σ distortion in x and y are still

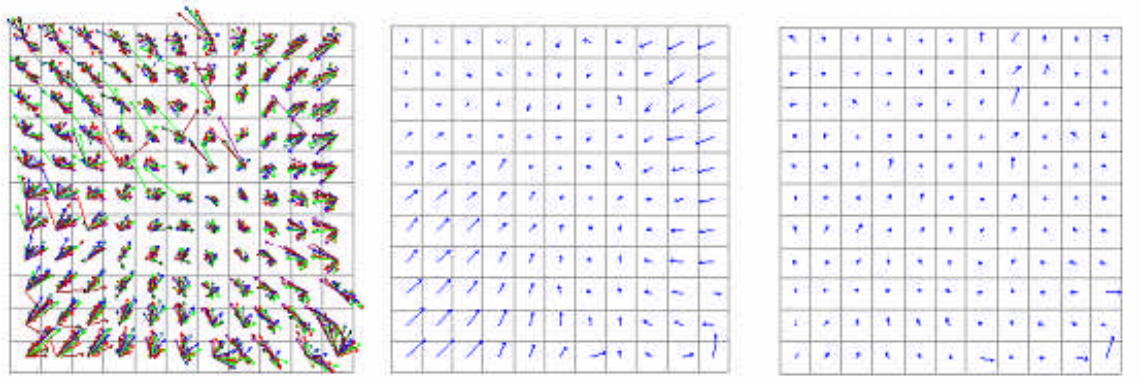

Summary	X[nm]	Y[nm]	Summary	X[nm]	Y[nm]	Summary	X[nm]	Y[nm]
Mean	-0.00	4.91	**Mean**	0.00	4.91	**Mean**	0.00	4.91
Max 3 S.D.	64.60	57.03	**Max 3 S.D.**	35.07	27.72	**Max 3 S.D.**	14.98	12.63
Min	-57.98	-37.28	**Min**	-23.89	-13.38	**Min**	-8.73	-3.45
Max	50.16	83.56	**Max**	26.97	30.96	**Max**	20.93	28.01

Figure 7. (a) Composite distortion map of all 27 fields, (b) average distortion map (a), and (c) average distortion map of 27 fields after first order error corrections

no greater than 15nm. Also, there are a small number of isolated points with somewhat higher local-distortion errors (e.g. the right lower corner of the 11x11 grid). The potential source of these isolated errors was not properly identified in this research, but can be due to a variety of factors including poorly defined placement marks leading to inferior metrology or local back side particles in the template chuck. The overall scaling difference between the x and y axes of the template before and after post-processing was therefore almost identical (0.434ppm for the template and 0.430ppm for the averaged map of Figure 7(b)).

4. First order (magnification and orthogonality) error corrections

For the purpose of first order corrections for S-FIL process, a multi-point forcing mechanism was developed that can induce optimized vectors of correction forces along the periphery of the template. Figure 8 shows experimental results of the stress distribution of a photo-elastic plate to ensure that uniform normal stresses are imparted to the active area without any significant in-plane distortions. A photo-elastic plate displays color changes associated with differential strains. When unidirectional mag forces are applied to the photo-elastic plate, stress distribution should be observed as color variations that are substantially uniform in the active

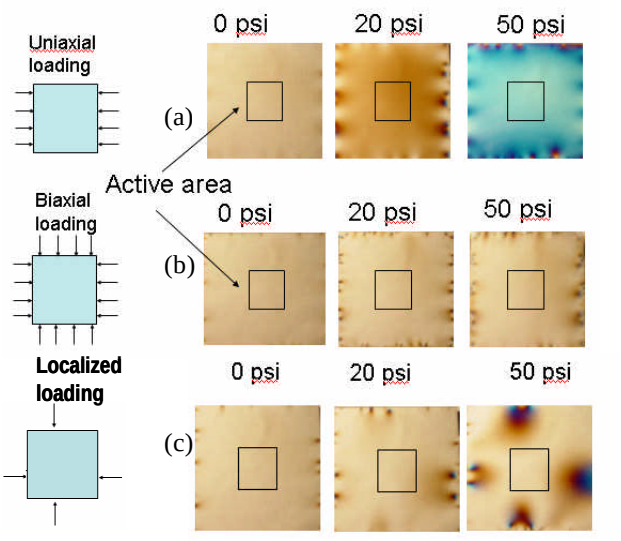

Figure 8. (a) Uniaxial mag, (b) biaxial mag, (c) local correction using photo-elastic plates shows uniform colors (strain fields) in the active area.

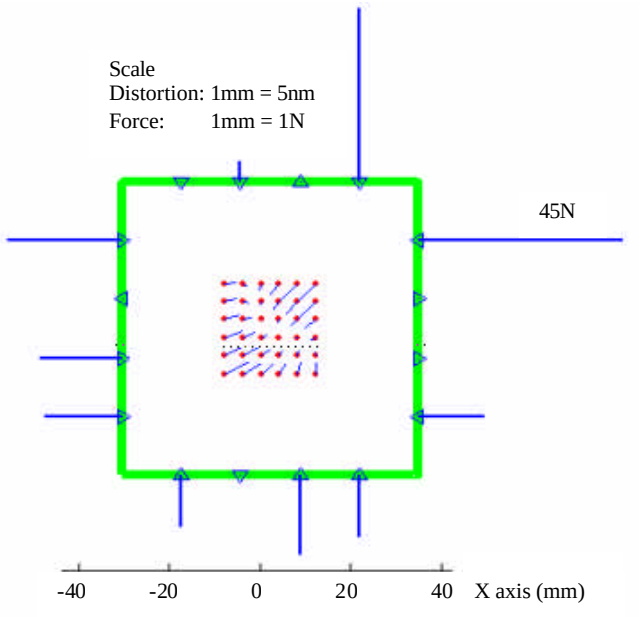

area. When biaxial mag forces are applied, if uniform mag is induced in both directions, no color change should appear in the active area. As seen in Figure 8, the magnification mechanism induces uniform unidirectional and bi-directional magnification control. In 8(c), it is also seen that a highly localized scaling, which represents an extreme case of non-uniform mag correction, leads to uniform strains in the active area.

Figure 9 shows an optimized force layout for the 1st order compensation (mag and orthogonality compensations) and a corresponding correction map. It is assumed that the template IPD data is known in advance for the processing and the correction mechanism can adjust the applied force vector. A simple min-max scheme was implemented with three equal constraints; $\Sigma f_x = 0$, $\Sigma f_y = 0$ and $\Sigma M_z = 0$ and a 16×1 vector unequal constraints; $f_i >= 0$. Original error of ~28nm 3σ was decreased to ~15nm 3σ according to this optimization.

5. X,Y, Q alignment scheme and experimental data

The S-FIL technology makes use of field-by-field in-liquid "through the template" alignment. Since the template and the substrate are separated by a thin film of liquid monomer during the alignment process, there is no problem of "sticking" during the alignment process. Advantages of an in-situ liquid alignment are several, including nanometer-scale alignment correction capability, in-situ correction just prior to UV-exposure with "locking" of the alignment. An example of the capability exhibited to date shows sub-10nm alignment, 3σ (Figure 10). It is expected that improvements in temperature control should lead to further improved results.

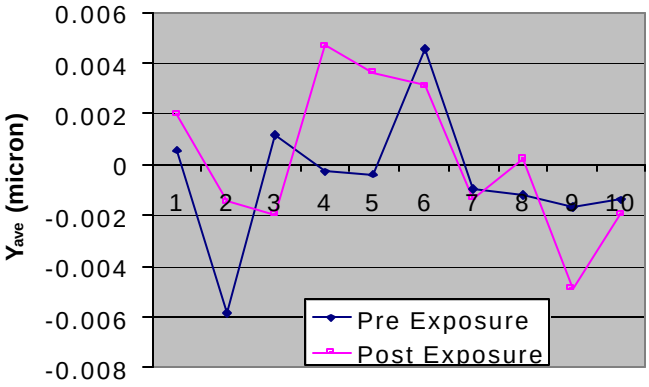

Figure 10. In liquid alignment – pre- and post-exposure

6. Summary

This paper focused on various sources of distortion and their contributions to the overlay errors in the S-FIL process. A summary of the major sources of overlay errors (3σ) is provided below:

- Alignment and magnification control error: **~10 nm**, 3σ
- Template e-beam placement accuracy? ~15 nm, 3σ
- Post-processing template placement accuracy?
    - Raw data (dominated by orthogonality errors) 35 nm, 3σ
    - Corrected for first order effects **15 nm**, 3σ
- Wafer-to-wafer process distortion?

- Raw data (dominated by environmental thermal scaling) upto 50 nm, (m+3σ)
- Corrected for thermal scaling **18 nm**, 3σ

Since the template IPD error includes the e-beam placement error, the total overlay estimate is $10+(15^2+18^2)^{1/2} = 33$(nm). The first one is a first order alignment error that is added linearly while the second and third errors are independent distortions that are assumed to be quadratically added. Thermal effect can be fairly well maintained with a proper environmental control unit (ECU) while the 1st order compensation requires for unique correction mechanism(s) as compared to other lithography processes. Assuming that there is a practical limit in such a correction function, the total overlay estimate is $10+(35^2+18^2)^{1/2} = 50$(nm).

7. Future work

In order to further improve the overlay performance of the S-FIL process, the following key challenges need to be addressed further:

- Template issues
  - Reduce e-beam pattern distortion
  - Understand source of errors during template post-processing
- Tool issues
  - Integration of first order corrections
  - Improved tool temperature control
- All other process distortions

Acknowledgements

This work was partially supported by grants from the DARPA Advanced Lithography program (Grants No. N66001-01-1-8964 and N66001-02-C-8011). The authors would also like to

acknowledge the technical support provided by Dupont Photomasks, Inc. for template fabrication and metrology.

References

1. S.Y. Chou, et al, J. Vac. Sci. Technol. B 15(6) (1997) 2897-2904

2. M. Colburn, et al, Proc. of SPIE 3676 (1999) 379-389

3. M. Bender, et al, Microelectronic Eng. 53 (2000) 233

4. I. McMackin, et al, Proc. Of SPIE, vol. 5037 (2003) 178-186

5. C. Perret, et al, Microelectronic Eng. 73-74 (2004) 172-177

6. D. J. Resnick, et al., Proc. of SPIE, vol. 4688, 2002.

7. K. J. Nordquist, et al, BACUS 2002, Monterey, CA

8. C. Martin, et al, EIPBN Conference, June 2002

9. A. Y. Abdo, et al, Microelectronic Eng. 73-74 (2004) 161-166

10. R. L. Engelstad, et al, Microelectronic Eng. 73-74 (2004) 904-909